Title

In vivo volumetric imaging of human retinal circulation with phase-variance optical coherence tomography

Journal

Biomedical Optics Express, 2(6)

ISSN

2156-7085

Authors

Kim, Dae Yu
Fingler, Jeff
Werner, John S
et al.

Publication Date

2011-06-01

DOI

10.1364/boe.2.001504

Peer reviewed

In vivo volumetric imaging of human retinal circulation with phase-variance optical coherence tomography

Dae Yu Kim,[1,2] Jeff Fingler,[3] John S. Werner,[1,2] Daniel M. Schwartz,[4] Scott E. Fraser,[3] and Robert J. Zawadzki[1,*]

[1]*Department of Ophthalmology & Vision Science, University of California Davis, Davis, CA 95616, USA*
[2]*Department of Biomedical Engineering, University of California Davis, Davis, CA 95616, USA*
[3]*Department of Biology, California Institute of Technology, Pasadena, CA 91125, USA*
[4]*Department of Ophthalmology, University of California San Francisco, San Francisco, CA 94143, USA*
**rjzawadzki@ucdavis.edu*

Abstract: We present *in vivo* volumetric images of human retinal micro-circulation using Fourier-domain optical coherence tomography (Fd-OCT) with the phase-variance based motion contrast method. Currently fundus fluorescein angiography (FA) is the standard technique in clinical settings for visualizing blood circulation of the retina. High contrast imaging of retinal vasculature is achieved by injection of a fluorescein dye into the systemic circulation. We previously reported phase-variance optical coherence tomography (pvOCT) as an alternative and non-invasive technique to image human retinal capillaries. In contrast to FA, pvOCT allows not only noninvasive visualization of a two-dimensional retinal perfusion map but also volumetric morphology of retinal microvasculature with high sensitivity. In this paper we report high-speed acquisition at 125 kHz A-scans with pvOCT to reduce motion artifacts and increase the scanning area when compared with previous reports. Two scanning schemes with different sampling densities and scanning areas are evaluated to find optimal parameters for high acquisition speed *in vivo* imaging. In order to evaluate this technique, we compare pvOCT capillary imaging at 3x3 mm^2 and 1.5x1.5 mm^2 with fundus FA for a normal human subject. Additionally, a volumetric view of retinal capillaries and a stitched image acquired with ten 3x3 mm^2 pvOCT sub-volumes are presented. Visualization of retinal vasculature with pvOCT has potential for diagnosis of retinal vascular diseases.

OCIS codes: (110.4500) Optical coherence tomography; (170.0110) Imaging systems; (170.4470) Ophthalmology; (120.3890) Medical optics instrumentation

References and links

1. D. Huang, E. A. Swanson, C. P. Lin, J. S. Schuman, W. G. Stinson, W. Chang, M. R. Hee, T. Flotte, K. Gregory, C. A. Puliafito, and J. G. Fujimoto, "Optical coherence tomography," Science **254**(5035), 1178–1181 (1991).
2. A. F. Fercher, C. K. Hitzenberger, W. Drexler, G. Kamp, and H. Sattmann, "In vivo optical coherence tomography," Am. J. Ophthalmol. **116**(1), 113–114 (1993).
3. L. An, H. M. Subhush, D. J. Wilson, and R. K. Wang, "High-resolution wide-field imaging of retinal and choroidal blood perfusion with optical microangiography," J. Biomed. Opt. **15**(2), 026011 (2010).
4. L. Yu and Z. Chen, "Doppler variance imaging for three-dimensional retina and choroid angiography," J. Biomed. Opt. **15**(1), 016029 (2010).
5. T. Schmoll, C. Kolbitsch, and R. A. Leitgeb, "Ultra-high-speed volumetric tomography of human retinal blood flow," Opt. Express **17**(5), 4166–4176 (2009).
6. Y. K. Tao, K. M. Kennedy, and J. A. Izatt, "Velocity-resolved 3D retinal microvessel imaging using single-pass flow imaging spectral domain optical coherence tomography," Opt. Express **17**(5), 4177–4188 (2009).
7. A. Szkulmowska, M. Szkulmowski, D. Szlag, A. Kowalczyk, and M. Wojtkowski, "Three-dimensional quantitative imaging of retinal and choroidal blood flow velocity using joint Spectral and Time domain Optical Coherence Tomography," Opt. Express **17**(13), 10584–10598 (2009).

#143864 - $15.00 USD Received 14 Mar 2011; revised 9 May 2011; accepted 27 Apr 2011; published 11 May 2011

8. S. Makita, T. Fabritius, and Y. Yasuno, "Quantitative retinal-blood flow measurement with three-dimensional vessel geometry determination using ultrahigh-resolution Doppler optical coherence angiography," Opt. Lett. **33**(8), 836–838 (2008).
9. M. Wojtkowski, R. Leitgeb, A. Kowalczyk, T. Bajraszewski, and A. F. Fercher, "In vivo human retinal imaging by Fourier domain optical coherence tomography," J. Biomed. Opt. **7**(3), 457–463 (2002).
10. J. Fingler, D. Schwartz, C. Yang, and S. E. Fraser, "Mobility and transverse flow visualization using phase variance contrast with spectral domain optical coherence tomography," Opt. Express **15**(20), 12636–12653 (2007).
11. J. Fingler, C. Readhead, D. M. Schwartz, and S. E. Fraser, "Phase-contrast OCT imaging of transverse flows in the mouse retina and choroid," Invest. Ophthalmol. Vis. Sci. **49**(11), 5055–5059 (2008).
12. J. Fingler, R. J. Zawadzki, J. S. Werner, D. Schwartz, and S. E. Fraser, "Volumetric microvascular imaging of human retina using optical coherence tomography with a novel motion contrast technique," Opt. Express **17**(24), 22190–22200 (2009).
13. A. M. Joussen, T. W. Gardner, B. Kirchhof, and S. J. Ryan, *Retinal Vascular Disease* (Springer, 2007).
14. D. A. Dartt, J. Besharse, and R. Dana, *Encyclopedia of the Eye* (Elsevier, 2010).
15. F. Musa, W. J. Muen, R. Hancock, and D. Clark, "Adverse effects of fluorescein angiography in hypertensive and elderly patients," Acta Ophthalmol. Scand. **84**(6), 740–742 (2006).
16. X. J. Wang, T. E. Milner, and J. S. Nelson, "Characterization of fluid flow velocity by optical Doppler tomography," Opt. Lett. **20**(11), 1337–1339 (1995).
17. Z. Chen, T. E. Milner, S. Srinivas, X. Wang, A. Malekafzali, M. J. C. van Gemert, and J. S. Nelson, "Noninvasive imaging of in vivo blood flow velocity using optical Doppler tomography," Opt. Lett. **22**(14), 1119–1121 (1997).
18. J. A. Izatt, M. D. Kulkarni, S. Yazdanfar, J. K. Barton, and A. J. Welch, "In vivo bidirectional color Doppler flow imaging of picoliter blood volumes using optical coherence tomography," Opt. Lett. **22**(18), 1439–1441 (1997).
19. V. Yang, M. Gordon, B. Qi, J. Pekar, S. Lo, E. Seng-Yue, A. Mok, B. Wilson, and I. Vitkin, "High speed, wide velocity dynamic range Doppler optical coherence tomography (Part I): System design, signal processing, and performance," Opt. Express **11**(7), 794–809 (2003).
20. R. Leitgeb, L. Schmetterer, W. Drexler, A. Fercher, R. Zawadzki, and T. Bajraszewski, "Real-time assessment of retinal blood flow with ultrafast acquisition by color Doppler Fourier domain optical coherence tomography," Opt. Express **11**(23), 3116–3121 (2003).
21. B. White, M. Pierce, N. Nassif, B. Cense, B. Park, G. Tearney, B. Bouma, T. Chen, and J. de Boer, "In vivo dynamic human retinal blood flow imaging using ultra-high-speed spectral domain optical coherence tomography," Opt. Express **11**(25), 3490–3497 (2003).
22. S. Makita, Y. Hong, M. Yamanari, T. Yatagai, and Y. Yasuno, "Optical coherence angiography," Opt. Express **14**(17), 7821–7840 (2006).
23. A. H. Bachmann, M. L. Villiger, C. Blatter, T. Lasser, and R. A. Leitgeb, "Resonant Doppler flow imaging and optical vivisection of retinal blood vessels," Opt. Express **15**(2), 408–422 (2007).
24. M. Szkulmowski, A. Szkulmowska, T. Bajraszewski, A. Kowalczyk, and M. Wojtkowski, "Flow velocity estimation using joint Spectral and Time domain Optical Coherence Tomography," Opt. Express **16**(9), 6008–6025 (2008).
25. L. An and R. K. Wang, "In vivo volumetric imaging of vascular perfusion within human retina and choroids with optical micro-angiography," Opt. Express **16**(15), 11438–11452 (2008).
26. A. Mariampillai, B. A. Standish, E. H. Moriyama, M. Khurana, N. R. Munce, M. K. K. Leung, J. Jiang, A. Cable, B. C. Wilson, I. A. Vitkin, and V. X. D. Yang, "Speckle variance detection of microvasculature using swept-source optical coherence tomography," Opt. Lett. **33**(13), 1530–1532 (2008).
27. B. J. Vakoc, R. M. Lanning, J. A. Tyrrell, T. P. Padera, L. A. Bartlett, T. Stylianopoulos, L. L. Munn, G. J. Tearney, D. Fukumura, R. K. Jain, and B. E. Bouma, "Three-dimensional microscopy of the tumor microenvironment in vivo using optical frequency domain imaging," Nat. Med. **15**(10), 1219–1223 (2009).
28. S. Zotter, M. Pircher, T. Torzicky, M. Bonesi, E. Götzinger, R. A. Leitgeb, and C. K. Hitzenberger, "Visualization of microvasculature by dual-beam phase-resolved Doppler optical coherence tomography," Opt. Express **19**(2), 1217–1227 (2011).
29. S. Makita, F. Jaillon, M. Yamanari, M. Miura, and Y. Yasuno, "Comprehensive in vivo micro-vascular imaging of the human eye by dual-beam-scan Doppler optical coherence angiography," Opt. Express **19**(2), 1271–1283 (2011).
30. D. Y. Kim, J. S. Werner, and R. J. Zawadzki, "Comparison of phase-shifting techniques for in vivo full-range, high-speed Fourier-domain optical coherence tomography," J. Biomed. Opt. **15**(5), 056011 (2010).
31. N. Nassif, B. Cense, B. Park, M. Pierce, S. Yun, B. Bouma, G. Tearney, T. Chen, and J. de Boer, "In vivo high-resolution video-rate spectral-domain optical coherence tomography of the human retina and optic nerve," Opt. Express **12**(3), 367–376 (2004).
32. R. J. Zawadzki, S. M. Jones, S. S. Olivier, M. Zhao, B. A. Bower, J. A. Izatt, S. Choi, S. Laut, and J. S. Werner, "Adaptive-optics optical coherence tomography for high-resolution and high-speed 3D retinal in vivo imaging," Opt. Express **13**(21), 8532–8546 (2005).
33. M. Wojtkowski, V. Srinivasan, T. Ko, J. Fujimoto, A. Kowalczyk, and J. Duker, "Ultrahigh-resolution, high-speed, Fourier domain optical coherence tomography and methods for dispersion compensation," Opt. Express **12**(11), 2404–2422 (2004).

#143864 - $15.00 USD Received 14 Mar 2011; revised 9 May 2011; accepted 27 Apr 2011; published 11 May 2011

1. Introduction

At present, the most widely used technique for examining the circulation of the retina in clinical settings is fundus fluorescein angiography (FA). This is a procedure in which the fundus is photographed through a bandpass filter following excitation of an extrinsic fluorophore, fluoroscein sodium (a compound that fluoresces after absorbing short-wavelength light) as it is injected into the blood stream through a vein. In an effort to replace this invasive procedure, one commercial system (Retinal Functional Imager, Optical Imaging) has been developed to image retinal vasculature without use of any extrinsic contrast agents using a fundus camera. In this paper we concentrate on optical coherence tomography (OCT) [1,2] methods that have the benefit of offering perfusion maps or flow with depth information in the human retina [3–8]. The phase-variance based motion contrast technique for Fourier-domain OCT (Fd-OCT) [9] has been implemented successfully in visualizing vasculature of the zebrafish [10], ocular circulation of the mouse [11], and human retinal vasculature [12].

Visualization of the retinal vasculature and microcirculation is essential for clinical diagnostics and treatment monitoring of retinal vascular diseases. The primary function of capillaries in the eye is to supply nutrients, exchange respiratory gases, and to excrete byproducts of metabolic reactions in the retina. Ocular vascular diseases transform the morphology of vessels and the formation of capillary networks, angiogenesis and vaso-occlusions caused by vascular endothelial cell aging, and damage associated with lifestyle-related illnesses such as diabetes mellitus, hypertension, and heart disease. In the human retina, there are generally three specific layers with capillary networks. The major arterial and venous branches are present in the nerve fiber layer or the ganglion cell layer. In addition, two capillary branches of the intermediate plexus and the deeper plexus are located in between the inner plexiform layer and the inner nuclear layer as well as between the outer plexiform layer and the outer nuclear layer, respectively [13]. In histology, the lumen diameter of human retinal vessels has approximately ~100 μm of arteries and ~200 μm of veins close to the optic disk and ~15 μm of microcapillaries in the deeper retina [14]. In a clinical environment, fundus FA generates vasculature maps of the retina and blood stream flow for identification of arteries and veins as well as hemorrhage. Additionally, commercial system fundus FA supports relatively easy operation, fast capture, and high-resolution fundus images. In rare instances, however, FA may cause adverse reactions in patients who are hypertensive or elderly [15]. Moreover, patients may experience nausea, vomiting, or acute hypertension during or after fundus FA imaging.

In order to measure blood flow and dynamics, optical Doppler tomography [16] was developed to measure velocity profiles of fluid flow by detection of Doppler shifts. Doppler OCT demonstrated *in vivo* flow imaging of the rodent skin [17] and the directional color map of biological tissue [18]. Since then, a number of *in vivo* vasculature imaging techniques have been reported using variations of OCT including: Doppler Fd-OCT with the histogram-based method [19], color Doppler Fd-OCT [20], Doppler Fd-OCT with the bulk motion removal method [21], optical coherence angiography [22], resonant Doppler flow imaging [23], joint spectral and time domain OCT [24], optical micro-angiography [25], speckle variance OCT [26], Doppler optical frequency domain imaging [27], and dual-beam Doppler OCT [28,29]. Phase-variance optical coherence tomography (pvOCT) identifies regions of motion between consecutive B-scans, which allows mapping of micro-vasculature without quantitative flow information [12].

In this paper we present contrast agent free images of *in vivo* human retinal vasculature using phase-variance based motion contrast OCT. High-speed image acquisition at 125,000 A-scans/s, compared to previously reported 25,000 A-scans/s [12], allows a dramatic decrease of motion artifacts and increases the field of view that can be imaged within a few seconds in a single volume acquisition. To visualize capillaries in two- and three-dimensions, two scanning patterns are used with different sampling densities and scanning areas including 3x3 mm^2 and 1.5x1.5 mm^2. The processed data show depth-resolved retinal micro-vascular maps for different field sizes and total acquisition times. Furthermore, two-dimensional phase-

#143864 - $15.00 USD Received 14 Mar 2011; revised 9 May 2011; accepted 27 Apr 2011; published 11 May 2011

variance data over a selected depth region as well as three-dimensional representation of the vasculature are presented and compared with fundus FA images.

2. Materials and methods

2.1. Phase-variance optical coherence tomography instrument

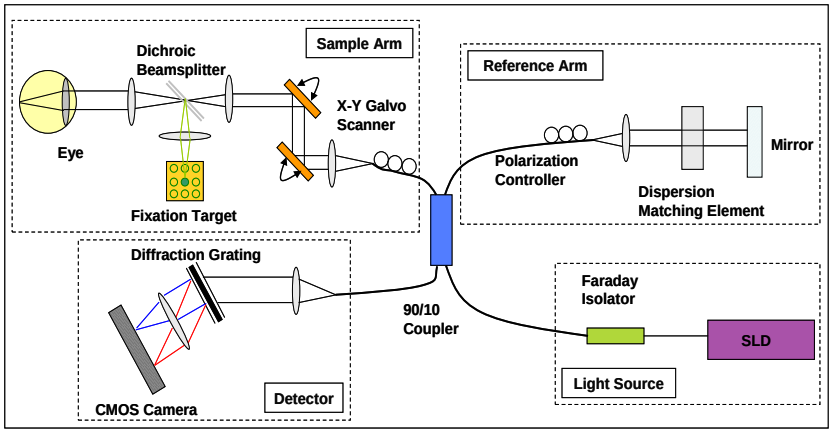

Fig. 1. Schematic of the Fourier-domain OCT instrument. The CMOS (Complementary Metal Oxide Semiconductor) camera is driven by a LabVIEW operating program on a workstation computer through a frame grabber. Subjects can see a green dot from the fixation target through the dichroic beamsplitter. SLD: Superluminescent diode.

Figure 1 is a schematic of the Fourier-domain OCT system with the CMOS (Complementary Metal Oxide Semiconductor) line detector [30] used to acquire data presented in this paper. A superluminescent diode (Superlum, Ireland) with an 855 nm central wavelength and a full width half maximum of 75 nm is used as a light source. The axial resolution is 4.5 μm in the retina (refractive index, n = 1.38). The lateral resolution of the system at the retina is estimated at 10 μm to 15 μm depending on the subject's ocular aberrations. A standard fiber-based OCT instrument is operated in Michelson interferometer configuration, connecting the fiber coupler (OZ Optics, Ontario, Canada) with 90/10 splitting ratio. 10% of the input light is sent to the sample arm and the power of the imaging beam at the cornea is 350 μW. The remaining 90% of the light is sent toward the reference arm where it is back reflected by the mirror and passed to the detector arm where it interferes with the light back scattered from the sample. The reference arm length matches the sample arm length which is set by the position of the imaging sample. The resulting interference in the form of the spectral fringe pattern between the sample and the reference arm is detected in the custom-built spectrometer. The spectrometer consists of a 75 mm focal length collimating objective, a 1200 l/mm diffraction grating, and a 150 mm objective which focuses the light onto the CMOS detector (spL4096-140km, Basler). The maximum line rate of the detector is 140 kHz at 4096 pixels and 10x10 μm (dual line) pixel size. Configuration setups of the CMOS camera are 4-tap, 12-bit, 80-MHz camera link clocks; the line averaging mode, a 125 kHz line rate and 2048 active detector pixels. Subject's gaze is stabilized using a custom-built fixation target reflected through a dichroic beamsplitter (FF662-FDi01, Semrock). The fixation target is composed of an 8x8 LED (light emitting diode) matrix which emits 516 nm (green) light and an electronic controller to switch fixation light position. During acquisition with LabVIEW software (National Instruments), 3 to 5 seconds depending on scanning pattern settings, the raw data are stored in the workstation (HP xw8600, 3.2-GHz dual processors) with the rapid speed frame grabber (PCIe 1429, National Instruments).

2.2. Image acquisition and data processing

Fd-OCT data sets were acquired in the Vision Science and Advanced Retinal Imaging laboratory (VSRI) at the University of California Davis Medical Center on a 59-year-old

#143864 - $15.00 USD Received 14 Mar 2011; revised 9 May 2011; accepted 27 Apr 2011; published 11 May 2011

healthy subject with normal ocular media. Written informed consent approved by the institutional review board was obtained prior to imaging. The subject's head position was fixed during acquisition using a bite-bar and forehead rest. Pupil dilation was not needed for imaging. Scanning areas of the retina were 3x3 mm^2 and 1.5x1.5 mm^2, as shown in Figs. 2 (a) and (b), respectively. Multiple B-scans at the same position, referred to as a BM-scan, were used to acquire the phase-change measurements required for the phase-variance contrast. In the 3x3 mm^2 scanning pattern, spacing between successive A-scans was 6 μm and 15 μm between BM-scans. Five B-scans were acquired within each BM-scan, resulting in four phase changes for the variance calculation at each location. For the 1.5x1.5 mm^2 scanning scheme, 4 μm spacing between both consecutive A-scans and BM-scans was used. Due to the spatial oversampling between consecutive BM-scans, phase changes from within two adjacent BM-scans were used for the variance calculations. Three B-scans were acquired within each BM-scan in this case, producing two phase change measurements for each BM-scan. For this scan, phase-variance calculations utilize four phase changes from two adjacent BM-scans, allowing for identical statistics to the 3x3 mm^2 scan pattern. The A-line exposure time was 6.3 μs and the spectral data were saved in a tiff format for post-processing in LabVIEW software using standard Fd-OCT procedures including spectral shaping, zero-padding, and dispersion compensation [31–33]. All retinal images shown in this manuscript were acquired *in vivo* at 125,000 axial scans (A-scan) per second.

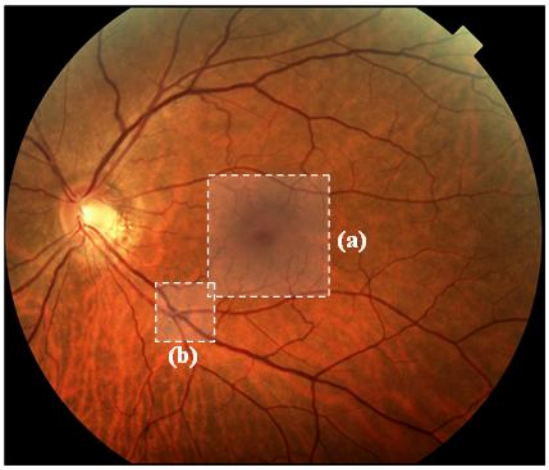

Fig. 2. Fundus color photograph of a normal human subject with OCT scanning locations. (a) Scanning 3x3 mm^2 of a parafoveal region. (b) Scanning 1.5x1.5 mm^2 of a perifoveal region.

As shown in Figs. 3 (a) and (b), the Fourier transform of spectral fringes (after remapping to k-space) from one B-scan acquired by the CMOS detector produces a complex OCT signal with intensity and phase information, respectively. Each B-scan consists of 500 A-scans acquired over 3 mm lateral scanning range. The dynamic range of the intensity image is 23 dB and the phase values vary from -π to + π. Note that one can discriminate retinal vessels, round shaped bright structures, in the ganglion cell layer from other retinal structures on the OCT B-scan in Fig. 3 (a). However, since the nerve fiber layer is highly scattering as well, a simple maximum projection view of the retinal layers doesn't provide sufficient contrast values for the retinal vessels. In the Fd-OCT, any particle movement will affect phase values of the acquired signal. The basic concept of motion detection relies on calculating phase differences of the same locations between consecutive B-scans by

$$\Delta\Phi_i(x,z,t) = \Phi_{i+1}(x,z,t+T) - \Phi_i(x,z,t) \qquad (1)$$

which can be interpreted as flow induced phase changes in the sample. Here, $\Phi_i(x,z,t)$ is the phase value in the B-scans at lateral location *x*, depth position z, time t, and T is the time

#143864 - $15.00 USD Received 14 Mar 2011; revised 9 May 2011; accepted 27 Apr 2011; published 11 May 2011

interval between two consecutive B-scans; *i* is an index of the *i*-th B-scan within one BM-scan. Then, the following variance calculation identifies mobility without quantitative flow information.

$$PhaseVariance = \frac{1}{N-1}\sum_{i=1}^{N-1}[\Delta\Phi_i(x,z,t) - \frac{1}{N-1}\sum_{i=1}^{N-1}\Delta\Phi_i(x,z,t)]^2 \qquad (2)$$

where *N* represents the number of B-scans used in the calculation. The preprocessed OCT data sets as seen in Figs. 3 (a) and (b) are then postprocessed by software developed at the Biological Imaging Center at the California Institute of Technology to extract phase-variance signals as shown on Fig. 3 (d). The cross-correlation function between consecutive intensity images aligns each B-scan from a BM-scan in an axial direction. Average intensity images and phase differences are calculated from sets of B-scans acquired at the same location. The image presented in Fig. 3 (c) results from averaging five B-scan intensity profiles, where one of the five B-scans is shown in Fig. 3 (a). Phase unwrapping is applied after obtaining the phase difference values. Additionally, bulk motion removal and histogram-based thresholding processing are implemented to remove phase shifts caused by eye motion. The phase-variance based motion contrast procedure generates B-scans of retinal motion information illustrated in Fig. 3 (d). The phase-variance data explained above is processed by an algorithm developed in LabVIEW programming software. The differences between results presented by Fingler et al. and this paper are primarily limited to changes in the scan patterns, which optimize the retinal scanning speed, and the implementation of a high speed CMOS line camera. Further details of the post-possessing algorithm and details are explained in the literature [12].

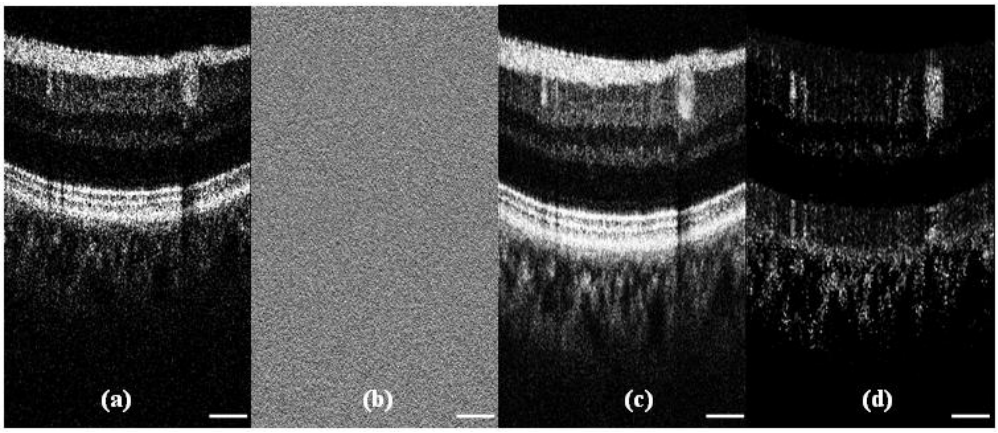

Fig. 3. Fourier domain optical coherence tomography of the *in vivo* human retina. (a) Intensity image of a single B-scan. (b) Phase image of the same single B-scan as (a). (c) Average intensity image of five B-scans. (d) Phase-variance processed image using phase data from the same five B-scans phase data as (c). The scanning size of the lateral direction is 3 mm and the sampling density of the lateral direction is 6 μm. Scale bar: 500 μm.

To visualize two- and three-dimensional vasculature networks in retinal layers, the three-dimensional phase-variance data sets are segmented from the nerve fiber layer to the outer nuclear layer. The *en face* projection view of the segmented data produces two-dimensional vascular perfusion maps which are similar to the ones obtained with fundus FA. The FA image (1280x1024 pixels) and the color fundus image shown in this paper were acquired with a Topcon (TRC-50IX) fundus camera. Moreover, pseudo-color (red-green-blue (RGB)) coding of the processed volumetric data sets was used to better visualize three-dimensional vessel networks and its projection view creates two-dimensional color vasculature imaging linearly scaled by axial location of the vessels.

#143864 - $15.00 USD Received 14 Mar 2011; revised 9 May 2011; accepted 27 Apr 2011; published 11 May 2011

3. Results and discussion

3.1. Retinal vascular network

The retinal vascular flow image shown in Fig. 4 (b) was reconstructed using a projection view of the retinal contributions of the phase-variance Fd-OCT data. The subject was imaged with FA and pvOCT on his left eye. This Fd-OCT volume was acquired over a 3x3 mm^2 retinal area captured in approximately 3.6 seconds. Figure 4 (a) shows the fundus FA image over the same region for comparison. Note that the phase-variance OCT image is similar to the fundus FA image, showing blood vessel networks of the retina. Arteries, vein branches, and relatively larger vessels are equally mapped by the two imaging techniques. pvOCT shows some of the micro-capillaries but sampling density in this scanning scheme is not sufficient to visualize all of them. High speed (125 kHz) imaging of the system allows shorter acquisition time, resulting in around 4.5 ms acquisition for each B-scan. This reduces imaging artifacts caused by involuntary eye motion. The last B-scan of this volumetric scan data set was used in Fig. 3.

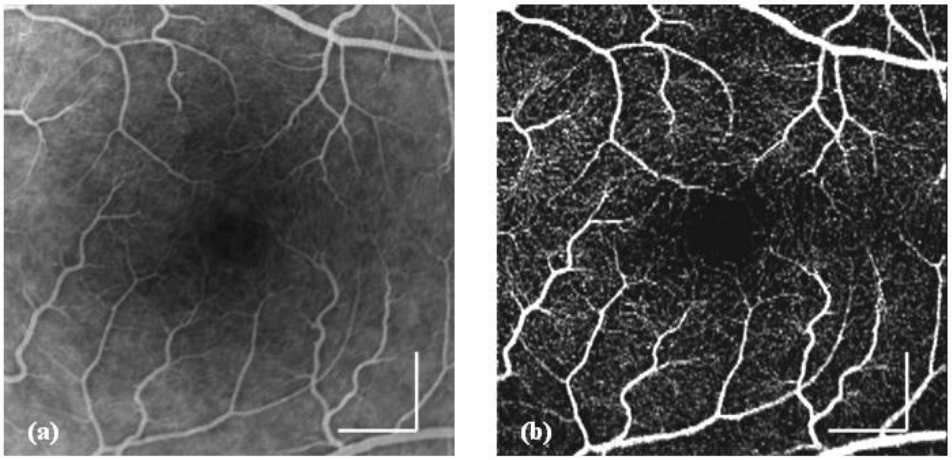

Fig. 4. *In vivo* human retinal vasculature images with a normal subject. The size of imaging is 3x3 mm^2. (a) Fluorescein angiography. (b) Projection image of phase-variance OCT retinal layers. The numbers of A-scans and B-scans are 500 and 200, respectively. The imaging acquisition time is 3.6 seconds. Scale bar: 500μm.

In order to reliably visualize micro-circulation, we used a scanning pattern with more densely sampled A-scans. In this pattern, sampling spacing is 4 μm between A-scans; BM-scans are acquired over a 1.5x1.5 mm^2 area of the human retina. Examples obtained with this acquisition scheme, including pvOCT reconstructed B-scans, are demonstrated in Fig. 5. Since the acquisition time of each B-scan is approximately 3.5 ms, we expect there is no significant eye motion between these scans. An average intensity image composed of three successive B-scans from a single BM-scan is shown in Fig. 5 (a). Moreover, Fig. 5 (b) shows the image post-processed with the phase-variance method from these data. The combined image with averaging intensity and phase variance, red color-coded is shown in Fig. 5 (c). The composite image validates that pvOCT identifies most of perfusion structures compared with the average intensity imaging where vessels can be classified by relatively bright structures. The video (Media 1) of the composite images is attached. Notice that there is a shadow artifact in the current phase-variance method that produces residual phase-variance values below vessels. This results in non-zero phase-variance values in retinal layers where non-perfusion should be observed including in the retinal pigmented epithelium.

Images illustrated in Fig. 6 are acquired over 1.5x1.5 mm^2 of the human perifoveal region. We compare maximum projection view of pvOCT in Fig. 6 (b) to the fundus FA in Fig. 6 (a), acquired at the same location. Figure 6 (b) shows dense micro-capillary networks, not distinctly recognizable in the zoomed fundus FA image. The size of the smallest

#143864 - $15.00 USD Received 14 Mar 2011; revised 9 May 2011; accepted 27 Apr 2011; published 11 May 2011

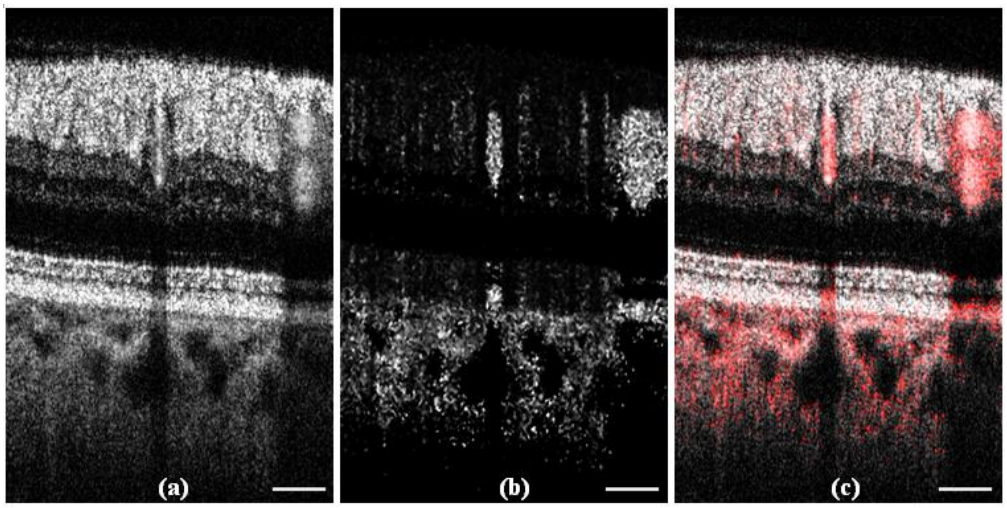

Fig. 5. Human retinal images of phase-variance OCT data processing over 1.5 mm. (a) Average intensity imaging of three B-scans from a single BM-scan. (b) Phase-variance image. (c) Combined image of average intensity (a) and red color-coded phase-variance imaging (b). Media 1 shows the composite image over the 1.5x1.5 mm^2 scanning area. The imaging acquisition time of a single BM-scan containing three B-scans is approximately 10 ms. Scale bar: 250 μm.

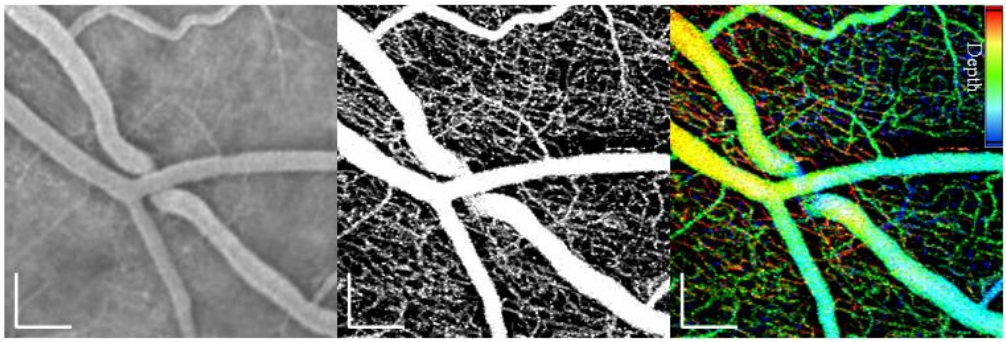

Fig. 6. *In vivo* human retinal micro-capillary network. Image size is 1.5x1.5 mm^2. (a) Fluorescein angiography. (b) Projection view of retinal contributions to pvOCT. The numbers of A-scans and B-scans are 375 and 360, respectively. (c) RGB depth color-coded projection view of retinal pvOCT data. Upper right shows depth scale bar with red color denoting a top layer, green showing capillaries as an intermediate vascular bed, and finally blue represents micro-capillaries as a deeper vascular plexus layer. The imaging acquisition time of pvOCT is 3.5 seconds. Scale bar: 250 μm. Media 2 shows C-scan fly through of the three-dimensional pvOCT data set.

resolvable capillary in this acquisition scheme is 10~12 μm. Since pvOCT includes depth information of capillary locations, Fig. 6 (c) shows a depth color-coded projection view. The pseudo-color (RGB) map codes the linearly-scaled axial location of the vessels. The superficial capillary network, here mostly within the nerve fiber layer or the ganglion cell layer, is coded as red. In addition, the intermediate capillary plexus, between the inner plexiform layer and the inner nuclear layer, is denoted by green. Finally, the deeper vascular plexus located in between the outer plexiform layer and the outer nuclear layer is colored as blue. The attached gray-scaled video (Media 2) demonstrates depth information of the vasculature using the pvOCT data set from the nerve fiber layer to the outer nuclear layer. The last B-scan of this volumetric data set was used in Fig. 5.

#143864 - $15.00 USD Received 14 Mar 2011; revised 9 May 2011; accepted 27 Apr 2011; published 11 May 2011

Figure 7 shows three-dimensional visualization of depth color-coded image of pvOCT from Fig. 6 (c). This image shows volumetric information of the vessel network at the perifoveal region in the human retina. Note again that the red-colored, larger diameter capillaries have green colored shadows underneath. This is because the pvOCT method creates the shadow artifact (non-zero phase-variance values) below relatively large vessels.

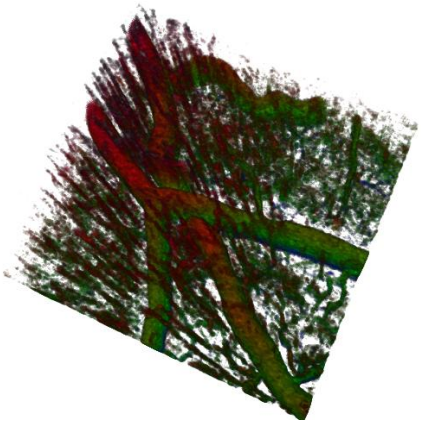

Fig. 7. Three-dimensional depth color-coded image of pvOCT, using the same data presented in Fig. 6 (c).

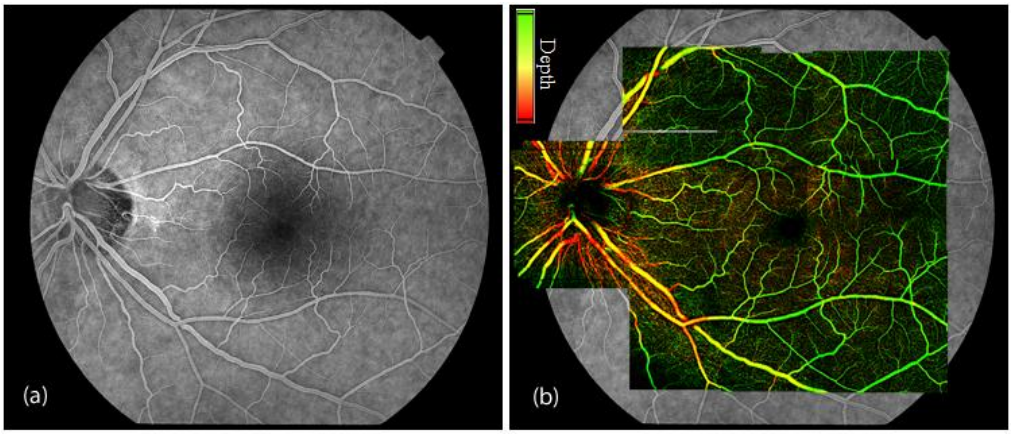

Fig. 8. Large field of view stitched pvOCT imaging overlaid on a fundus FA. (a) Fluorescein angiography. (b) Depth color-coded imaging with the ten volumes. Total image acquisition time for ten volumetric images is approximately 35 seconds.

To achieve a clinically applicable imaging method, the capability to image a large field of view is critical. However, the scanning patterns and the acquisition speed presented in this paper do not allow for larger than the 3x3 mm^2 scanning area. This was because of the need to maintain high-resolution with acquisition time in a single volume of a few seconds. To overcome this limitation, we acquired several volumes centered at different retinal locations. Figure 8 shows an example of the large field of view image overlaid on the fundus FA. This image was made from ten 3x3 mm^2 pvOCT volumes acquired by shifting the position of LED fixation points. After pvOCT processing, each projection image was manually aligned with linear translation to create a large field of view mosaic. The depth color-coded imaging in Fig. 8 (b) approximately segmented vessels from below the inner limiting membrane to the inner nuclear membrane as a green color as well as from below the inner nuclear membrane to the outer limiting membrane as a red color. Moreover, vasculature located in the intermediate

#143864 - $15.00 USD Received 14 Mar 2011; revised 9 May 2011; accepted 27 Apr 2011; published 11 May 2011

layer or laid across two layers segmented above has a yellowish color. The total time of ten images for acquisition only is 35 seconds.

4. Conclusions

We demonstrate feasibility of a high-speed phase-variance OCT system for two-dimensional visualization of the capillary network over foveal and perifoveal regions, as well as three-dimensional representation of the vasculature in the human retina. *En face* visualization of the human foveal area with pvOCT produces details of capillary networks comparable to fundus FA imaging without using any contrast agents. In addition, densely scanning a small field of view, 1.5x1.5 mm^2, generates the microcapillary perfusion map and color-coded depth information of the microvasculature. pvOCT with rapid image acquisition at an A-scan speed of 125 kHz reduces acquisition time, hence decreasing eye motion artifacts and producing larger field of view imaging. To demonstrate the feasibility of this technique for clinical applications, we showed the stitched vascular map of the retina acquired from multiple volumes. Our data suggest that pvOCT has potential in the early diagnosis of retinal vascular diseases including diabetic retinopathy and vascular-related macular degeneration. As further improvements, shadow artifacts will be minimized and high-resolution microcapillary networks of larger scanning areas will be visualized.

Acknowledgments

The authors thank Suman Pilli, Susan Garcia from the Vision Science and Advanced Retinal Imaging Laboratory, Department of Ophthalmology & Vision Science at the UC Davis Medical Center for help with OCT data acquisition. This research was supported by the Howard Hughes Medical Institute (HHMI) Med-into-Grad Initiative (HHMI-MIG 56006769), National Eye Institute (EY 014743), Research to Prevent Blindness (RPB), Beckman Institute, and That Man May See Foundation.

#143864 - $15.00 USD Received 14 Mar 2011; revised 9 May 2011; accepted 27 Apr 2011; published 11 May 2011